Heliyon 10 (2024) e39671

Contents lists available at ScienceDirect

Heliyon

journal homepage: www.cell.com/heliyon

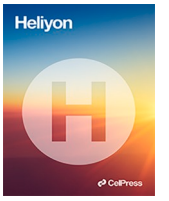

Research article

The impact of carbon quantum dots derived from spent coffee grounds on the droplet combustion of diesel/n-butanol blend

C. Zapata-Hernandez, G. Durango-Giraldo, Miguel Gomez-Echeverri, R. Buitrago-Sierra, Bernardo Herrera, Karen Cacua *

Group of Advanced Materials and Energy, Faculty of Engineering, Instituto Tecnológico Metropolitano, Street 54A No 30-01, Medellín, 050536, Colombia

ARTICLE INFO

Keywords:
Carbon quantum dots
CQD
Butanol
Droplet combustion
Fuel additives

ABSTRACT

As global concerns surrounding climate change mount and fossil fuel reserves diminish, the application of additives in internal combustion engines is increasingly prevalent. Butanol and carbonaceous nanomaterials, such as carbon quantum dots (CQD), are being employed as additives to increase engine efficiency and mitigate the emission of pollutants. Nevertheless, understanding the impact of these additives on combustion behavior at the droplet scale through combustion assessments before their use in engines is crucial. In this study, our main objective was to assess the impact of incorporating CQD dispersed in n-butanol as additives to conventional diesel fuel on the combustion characteristics at the droplet scale. CQD were obtained from spent coffee grounds (SCGs) using n-butanol as a solvent. The product obtained was mixed with Colombian commercial diesel (10 % vol. palm oil biodiesel), and its combustion was evaluated using the droplet combustion method. Before the CQD synthesis, SCGs were characterized by thermogravimetric analysis (TGA) and field emission scanning electron microscopy (FESEM). CQD were characterized via Fourier transform infrared (FTIR) spectroscopy, Transmission Electron Microscopy (TEM), UV–vis, and fluorescence spectroscopy. Results indicated that adding n-butanol and CQD to commercial diesel leads to a 5.4 % and 16.5 % increase in droplet ignition delay, respectively. These additives also cause droplet contraction and expansion cycles, resulting in unstable combustion. However, CQD reduces the frequency of microexplosions caused by boiling n-butanol inside the droplet, which mitigates instabilities during droplet combustion. Including CQD can enhance fuel evaporation by increasing the density of nucleation sites for bubble formation and preventing micro-explosions, thereby leading to stable combustion. These attributes can significantly influence the performance of blends in Compression Ignition (CI) Engines.

1. Introduction

Burning fossil fuels is a significant cause of environmental pollution, negatively impacting climate and human health. Since CI engines are an important source of pollutant emissions, particularly Particulate Matter (PM), recent research has focused on developing solutions that reduce these emissions while maintaining engine performance.

* Corresponding author.
E-mail address: karencacua@itm.edu.co (K. Cacua).

https://doi.org/10.1016/j.heliyon.2024.e39671
Received 20 March 2024; Received in revised form 7 June 2024; Accepted 21 October 2024
Available online 28 October 2024

After-treatment solutions, such as Diesel Oxidation Catalysts and Diesel Particulate Filters (DPF), are commonly used to meet emission standards and decrease the environmental impact of the engines. In addition to using nanomaterials as fuel additives, alternative fuels such as biodiesel and alcohols have also been proposed to reduce the emissions generated by CI engine [1]. Particularly, butanol produced through biological processes has a higher potential to reduce greenhouse gas emissions throughout its lifecycle [2].

For instance, lignocellulosic butanol has the potential to reduce greenhouse gas emissions by up to 60 % compared to diesel fuel. Blends of butanol and diesel, containing as much as 40 % butanol, could be effectively utilized in unmodified diesel engines calibrated for 100 % diesel [3]. Zang et al. [4] conducted a study that revealed that 20 % butanol by volume in diesel fuel resulted in a significant reduction of 62.05 % in soot emissions and a 7.34 % decrease in CO emissions compared to standard diesel. This favorable outcome was associated with the oxygen content of butanol, which was found to enhance combustion within the engine cylinder.

Butanol has a high cetane number and energy density compared to other alcohols with short carbon chains like methanol and ethanol. Because of its low polarity, it is possible to mix it with diesel without co-solvents [5]. Adding it to diesel can decrease soot emissions because of its oxygen content [6–8].

On the other hand, metal oxides (e.g., aluminum oxide, cerium oxide, and titanium oxide) and metals (e.g., copper, zinc, aluminum, and silver) have been incorporated as additives to diesel to enhance combustion processes owing to their catalytic properties [9,10]. For example, Firew et al. [11], utilized Nickel Zinc Iron Oxide ($NiZnFe_2O_4$) in a blend of diesel and ethanol (10 % vol), then tested this fuel in a diesel engine. They observed significant reductions in unburned hydrocarbons (UHC), carbon monoxide (CO), and smoke by 71 %, 81 %, and 61 %, respectively, when the nanoparticle concentration was 100 ppm. However, they noted that the NOx concentration increased by 33 % compared to standard diesel fuel.

Similarly, Pullagura et al. [12], studied the impact of adding SiO_2 nanoparticles to a fuel mix of 75 % diesel, 15 % Sea Mango Methyl Ester, and 10 % iso-butanol. Their findings showed that adding 60 mg/L of SiO_2 led to a 10.09 % improvement in brake thermal efficiency (BTE), a 17.4 % improvement in in-cylinder pressure (ICP), and a 10.73 % improvement in net heat release rate (NHRR). Additionally, there was a 19.13 % decrease in brake-specific fuel consumption (BSFC) and a significant reduction in hazardous pollutants, including carbon monoxide (CO) by 20.06 %, unburnt hydrocarbons (UHC) by 13.9 %, nitrogen oxides (NO_x) by 11.3 %, and smoke by 11.2 %. Cerium dioxide (CeO_2) [9] and aluminum oxide (Al_2O_3) [10] have been utilized in blends of diesel-alcohols with similar results.

Despite the positive results found using metal oxides and metals as additives to diesel fuel, there are concerns about the release of those types of nanoparticles into the environment and their potentially harmful effects [13]. To avoid this environmental impact, carbonaceous materials have emerged as a viable alternative to mitigate environmental and health concerns [14].

Materials like carbon nanotubes (CNTs), graphene oxide (GO), and, more recently, carbon quantum dots (CQD) have been dispersed in diesel and biodiesel blends to improve engine performance and reduce pollutant emissions [15,16].However, specific research is scarce in the academic literature on the effects of integrating CQD into diesel fuel on engine performance and emission parameters. Ettefaghi et al. [17], evaluated a mixture of diesel, biodiesel, and water as fuel in a CI engine, along with graphene quantum dots as additives. The results indicated that an engine using a fuel blend comprising 5 % water, 15 % biodiesel, and 60 ppm of nanoparticles experienced a 13.6 % increase in power and a 7.8 % reduction in brake-specific fuel consumption compared to a diesel-biodiesel blend with 15 % biodiesel. Additionally, NOx, HC, and soot emissions decreased by 3.8 %, 29.2 %, and 33.7 %, respectively.

Heidari-Maleni et al. [18], also used graphene quantum dot nanoparticles as an additive to diesel-biodiesel-ethanol blends. They evaluated the effect on the performance and emissions characteristics of a diesel engine. The addition of graphene quantum dots (90 ppm) to a mixture of diesel-biodiesel (10 %) and ethanol (6 %) improved the torque and power and decreased the specific fuel consumption, as well as CO, UHC, and NOx emissions.

The droplet combustion experiment is frequently used to understand better how alcohols and nanomaterials impact engine performance and emissions when used as additives in diesel or biodiesel-powered IC engines. This experimental method enables the identification and analysis of various mechanisms, including bubble dynamics, microexplosions, and secondary atomization, which can significantly impact engine performance and emissions. For instance, Degirmenci et al. [19] observed stable combustion and decreased ignition delay when blending methanol or ethanol with trimethyl borate in their study. On the other hand, the impact of boiling point differences of C1-C5 n-alcohols and polyoxymethylene dimethyl ether (PODE 4) or n-undecane on nucleation sites, bubble growth, coalescence, and droplet atomization was assessed using droplet scale combustion by Huang et al. [20]. Their evaluation revealed five atomization modes for the blends, varying bubble evolution, breakup, and droplet atomization.

According to the same authors, puffing, ejection, and microexplosion occur when the boiling point differences between binary droplets of PODEn (n = 1–4) and ethanol exceed 50 K [21]. Xi et al. [22], studied droplets of n-butanol and n-hexadecane as well as their blends. They found that droplets containing a single component go through transient heating and stable evaporation phases. In contrast, droplets containing binary mixtures exhibit three distinct phases during vaporization due to heterogeneous nucleation, especially when the proportion of n-butanol increases. Han et al. [23], examined the puffing and evaporation behavior of acetone-butanol-ethanol (ABE) and diesel blend droplets. They found that adding ABE to diesel led to droplet puffing, influencing evaporation. The evaporation of the ABE-diesel blend occurred in three distinct phases: the transient heating phase, the fluctuation evaporation phase, and the equilibrium evaporation phase.

In the study by Küçükosman et al. [24], an assessment was conducted on single and multicomponent fuels, which included both oxygenated and non-oxygenated fuels, at the droplet scale. The research revealed that the deformation mechanism was largely characterized by surface fluctuations and volumetric shape oscillations caused by droplet boiling. It was also noted that the boiling points and volatility of the fuels significantly impacted the duration of the preheating period.

Among the various nanomaterials utilized as fuel additives, CQD have significant properties such as thermal and electrical conductivity, large surface area, functionalities on their surface such as oxygen functional groups and distinctive physical and optical characteristics [25]. These nanomaterials can be obtained from various biomass wastes, including banana peel [26], bamboo wood [27], lychee exocarp [28], walnuts, and coffee residues [29].

Coffee waste, or the leftovers from the coffee brewing process, known as Spent Coffee Grounds (SCGs), has a significant potential for converting into high-value materials [30]. It is estimated that around 6 million tons of SCGs are produced annually worldwide [31], which has generated a growing interest in using them to create various products. In energy applications, SCGs have been used to produce SGCs oil, biodiesel, and bioethanol and used as solid fuel for direct combustion [32]; antioxidant and phenolic compounds have been extracted from SGCs using various methods.

These compounds are utilized in cancer treatments, skincare products, and as food antioxidants [30]. Bioactive compounds such as caffeine and chlorogenic acid are found in high abundance in SGCs obtained from diverse geographical regions across the globe. These compounds have numerous applications in the pharmaceutical, health, and cosmetic industries [33]. SGCs-based biorefineries have been assessed in various scenarios based on biorefinery size, design configuration, and location relative to the SGCs source [34].

Exploring the potential advantages of using CQD as a high-value product derived from SCGs offers a promising opportunity to improve diesel fuel combustion. Its size and oxygen functionalities make it an appealing additive to fuels. Additionally, n-butanol has demonstrated potential as an alternative fuel for reducing emissions, mainly PM in CI engines. Therefore, combining CQD and n-butanol as a compound additive could enhance engine performance and reduce emissions. This combination holds promise, as existing literature indicates positive outcomes when these additives are used individually in diesel.

This study synthesized carbon quantum dots (CQD) from spent coffee grounds using n-butanol as the solvent. The butanol-CQD blend was mixed with Colombian commercial diesel (10 % vol. palm oil biodiesel), and its combustion was studied at the droplet scale. The objective was to understand how these additives affect ignition delay and microexplosion frequency, critical combustion characteristics that can impact the combustion quality in a CI engine. This experiment represents the first attempt to evaluate diesel combustion with CQD-butanol additives from a phenomenological perspective.

2. Methodology

2.1. Synthesis and characterization of the SCGs and CQD

The CQD synthesis was carried out in two steps. In the first step, the fatty acids present in the SGCs were removed. Using the Soxhlet method, the SCGs were washed using 13 g of SCGs and 350 mL of acetone (Sigma Aldrich, 98 %). The SCGs were washed for 15 h at 60 °C to favor acetone evaporation. Then, the treated material was dried at 80 °C overnight. The CQD was synthesized at 200 °C for 2 h in the second step. For such purpose, 1.8 g of the previously treated SCGs were introduced into a stainless-steel autoclave reactor with 80 mL of 1-butanol (Panreac, 99.5 %). The obtained concentration of CQD in butanol was found to be 947 mg/L on average.

The morphology of the SCGs was evaluated using a Scanning Electron Microscope (JEOL JSM-7100F). The thermal stability was characterized by Thermogravimetric Analysis (TGA) using a Discovery TGA 550 (TA instruments). The sample was heated at 10 °C for 7 min until 800 °C under a nitrogen atmosphere. The atmosphere was then changed to air, and an isothermal treatment was applied for 15 min.

The concentration of CQDs on n-butanol was determined using the method described by Thulasi et al. [35]. Three beakers (50 mL) were weighed with a precise balance (WP 225SM-DR), and their initial weights were recorded. Subsequently, 25 mL of the CQDs solution was added to each beaker using a Volumetric balloon (25 mL). The solvent was evaporated entirely using an oven (Memmert HPP 110) at 80 °C, and the final weights of the beakers were recorded. The concentration of the CQDs was calculated using Equation X. This procedure was repeated three times, and the results indicated a concentration of 947.3 ± 40 mg/L.

$$[\text{CQDs}] = \frac{\text{Final beaker weight} - \text{Initial beaker weight}}{\text{Solution volume}} \quad (1)$$

The B10-Bu-CQD blend was prepared using 10 % Bu-CQD and 90 % commercial diesel. Initially, 0.3 mL of Bu-CQDs were measured using a Transferpette® S micropipette, and this volume was added to 2.7 mL of commercial diesel. The concentration of CQD on B10-Bu-CQD is 95 ± 4 mg/L.

The CQD in n-butanol were exposed to ultraviolet light (365 nm), and their morphology and size were analyzed using Transmission Electron Microscopy (TEM). TEM analysis was performed using a sample of butanol-CQD, which was diluted to a concentration of 0.01 wt%. Then, 5 μL was transferred to a grid (ultrathin carbon film supported by a copper grid, 400) using a Transferpette® S micropipette (Brand). The diameter of over 140 particles was measured using the open-source software Image J. The measurement process involved two steps: firstly, calibrating the TEM image to correlate pixel dimensions with physical dimensions, and secondly, using the software's tools to measure non-spherical particles, employing Feret's diameter to calculate their size [36]. The optical properties were evaluated using Ultraviolet–Visible spectroscopy (Agilent 8453), and their photoluminescence (PL) was examined using a fluorescence spectrophotometer (Duetta-Bio, Horiba). The functional groups in CQD were investigated using X-ray photoelectron spectroscopy (XPS) with PHOIBOS 150 1D-DLD and Fourier Transform Infrared (FTIR) spectrometer (IRTracer-100).

2.2. Droplet scale combustion

An examination of the evolution of droplet size over time using quantitative image processing is a suitable technique for

characterizing the burning of liquid fuel drops. A characteristic curve representing the variation of the normalized area (A/A_0) of the drop over time is shown in Fig. 1, obtained from the analysis of the combustion of a diesel-butanol-CQD droplet. This merely illustrative representation can be created by using frames taken from droplet combustion videos to analyze the variation of the droplet area. There are three main stages in the process of droplet combustion. The first stage involves the preheating and ignition of the droplet. The droplet's rapid thermal expansion characterizes the second stage. In the third stage, the droplet burns steadily or unsteadily [37]. Combustion features such as ignition delay (when the fuel starts burning) and steady and unsteady burning can be observed in each stage.

The experimental setup used to evaluate the droplet combustion is shown in Fig. 2. The combustion chamber was a cylindrical stainless-steel vessel measuring 280 mm in diameter and 280 mm in height. It featured two quartz windows for optical access and backlighting while operating at atmospheric conditions. The system comprises two electric resistances anchored to pneumatic cylinders, an infrared flame sensor, an ignition indicator (LED), a suspension element consisting of two crossed stainless-steel wires (diameter 0.2 mm), a backlight generated by an LED, and a high-speed camera (CHRONOS) along with two biconvex lenses.

Each experimental test begins with the addition of a drop of fuel (3 μL ± 0.05 μl) in the middle of the crossed wires, using a Transferpette® S micropipette (Brand). Subsequently, the pneumatic cylinders displace each electric resistance, which acts as the ignition system for the fuel drop. An Arduino UNO device was used for system control, which turns off an LED (ignition indicator) instantly when the resistances receive power to identify the ignition onset. Additionally, this device retracts the cylinders when the flame sensor detects combustion.

Biconvex lenses were used to collimate the light rays towards the sample and the camera lens, allowing the capture of images with defined contours. Therefore, the optical "shadowgraph" method was employed. This method is used to track the changes in the size of a droplet over time. This technique involves illuminating the droplet from behind and observing the refractive index difference at the interface between the droplet and its surroundings. The phenomenon occurs due to the light not contacting the droplet. The refracted light in contact with the droplet appears scattered, resulting in a darker appearance. This method is advantageous in studying the combustion of droplets in mediums with significantly differing refractive indices, such as air and diesel.

The experimental setup shown in Fig. 2 was designed to create shadowgraph images and comprises two main parts: the recording apparatus (a high-speed camera) and the light source. Using two biconvex lenses, the light beams are collimated towards the sample and the lens. This arrangement generates a uniform background on the recording sensor and provides the light that refracts off the sample.

2.3. Experimental design

The study involved an experimental evaluation using a random one-factor experimental design with three replicates. The response variables were the ignition delay (time between turning on the ignition source and the igniting point) and the microexplosion frequency. The treatments of the experimental design were built using two main variables: fuel type (diesel and a blend of diesel-butanol) and CQD concentration. The factor in this study was the fuel type, which had three treatments: commercial diesel (B10), a blend of commercial diesel and butanol (B10-Bu), and a blend of commercial diesel, butanol, and CQD. The details of every treatment are shown in Table 1. The order of preparation and analysis of the droplet combustion was determined randomly according to the one-factor experimental design method.

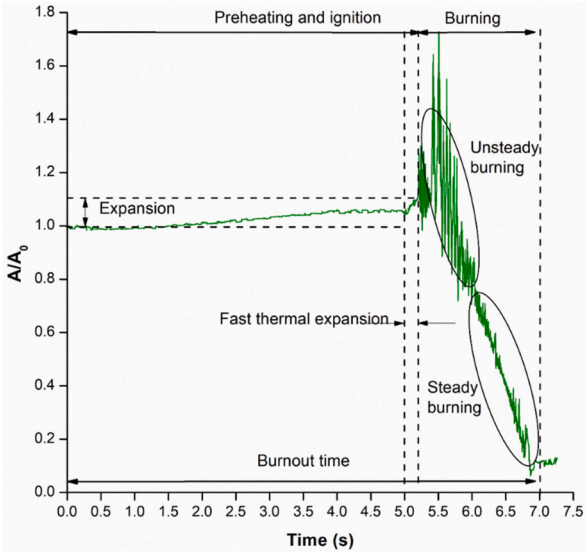

Fig. 1. The curve of variation of the normalized area during droplet combustion.

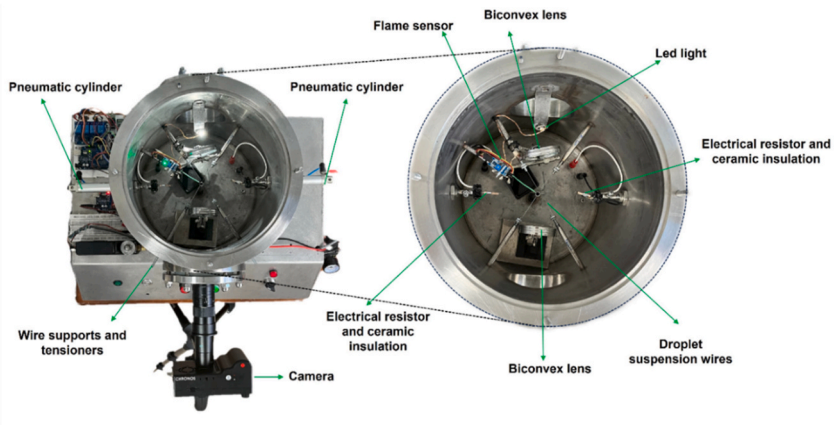

(a)

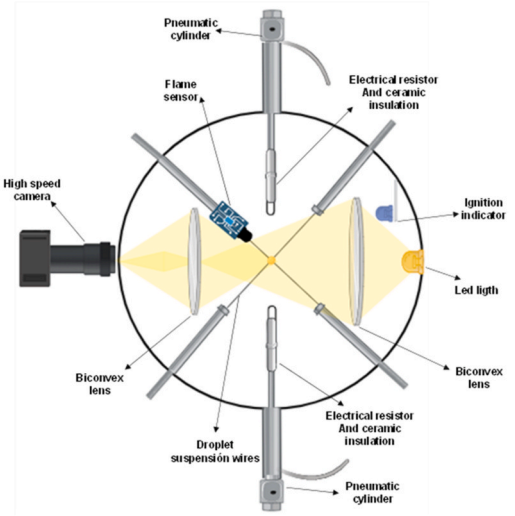

(b)

Fig. 2. Experimental setup to study the evolution of droplet combustion (a); Schematic diagram of the experimental setup (b).

2.4. Shadowgraph imaging

A high-speed camera, Chronos 1.4 CMOS with a 4/3-inch sensor, captured photographs of burning fuel drops. Each pixel has a pixel pitch of 6.6 μm. These capabilities allow for video recordings at 1280 x 1024 resolution with a frame rate of 1069 FPS, as high-quality pictures are necessary for post-processing. The photos in Fig. 3 display the burning of a B10 drop over 6.8 s, starting from 0 s. These photos can help us understand the combustion of the B10 drop in a non-quantitative way. The droplet initially takes the shape of a semi-circle, but its size and shape change as electrical resistances add heat, causing its volume to expand and temperature to rise. A combustion stage was then seen, and the ignition time coincided with the maximal volumetric expansion in around 5 s.

Table 1
Treatments of the one-factor experimental design.

Treatment	Concentration of B10	Concentration of Butanol	Concentration of CQD
1	100 %	0 %	0 mg/L
2	90 %	10 %	0 mg/L
3	90 %	10 %	95 mg/L

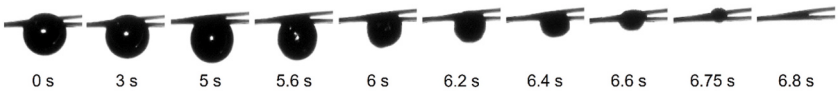

Fig. 3. Shadowgraph images extracted from a video of the combustion of a diesel-butanol droplet.

2.5. Post-processing of shadowgraph images

An algorithm was developed using MATLAB to track fuel droplet combustion. The algorithm extracts frames and creates characteristic curves (see Fig. 4).

Sequential pictures are read and written to accurately calculate droplet area and crop frames and extract FPS from droplet combustion videos. Our FPS extraction algorithm is designed to extract each frame from the video with precision. The combustion process typically takes 7–8 s, producing approximately 7900–7950 frames. To ensure consistency, we crop all images to 200x200 pixels with a resolution of 72x72 pixels per inch. Lastly, the droplet area is a selection of "on" pixels in a binarized image obtained by the Otsu method), returning it as a numerical scalar. Equation (2) was used to determine the normalized area (A/A_0), and the video frame rate was used to determine the time step.

$$A \Big/ A_0 = \frac{Area\ of\ binary\ image\ selected}{Initial\ droplet\ area} \tag{2}$$

2.6. Data reduction

Following Section 2.5, the area of the droplet was determined by counting the pixels in a binarized image. Consequently, our uncertainty analysis aligns with the methodologies outlined by Soudagar et al. [38] and Hussain et al. [39], relying solely on the standard deviation of the test. To conduct the experiment, the apparatus was used to ignite three droplets of each fuel. The normalized area ratio (A/A_0) curve was then calculated for each droplet over time using the procedure detailed in Section 2.5. The resulting curves were averaged, and the standard deviation of each time step was computed and represented as a shaded band around a solid line denoting the average (A/A_0).

Table 2 presents the minimum, maximum, and average coefficient of variation, which represents the ratio of the standard deviation to the mean, for the (A/A_0) ratio for each type of fuel. These three measurements are necessary because the standard deviation changes for each time step, and they offer an additional approach to quantifying the uncertainty of the normalized area.

The data in Table 2 indicates that the average coefficient of variation for all fuels is below 5 %. However, the blends containing butanol and CQD exhibited a maximum coefficient of variation greater than 50 %, indicating a significant level of uncertainty in estimating the ratio A/A_0 in such instances. This is primarily attributed to the substantial fluctuations of droplets during combustion caused by surface effects of butanol and CQD, as well as microexplosions resulting from the formation of bubbles inside the droplets, which will be further discussed.

The ignition delay does not have an associated uncertainty with a measurement device because it is assumed to be the time when the ratio A/A_0 is 95 % of the maximum ratio. This is because, according to Ooi et al. [37] and Wang et al. [40], the ignition time is established as the time where the maximum A/A_0 is achieved. However, in this study, the maximum A/A_0 occurs in a region where there is high fluctuation of the normalized droplet area. Therefore, we assumed that a better estimation of the ignition time was to take it as the time when the ratio A/A_0 is 95 % of the maximum ratio, following the criterium by Mosadegh et al. [41], who establish that ignition delay is the time difference between the instant that the heating starts and the instant when the normalized flame area reaches 0.95 of its global maximum, in order to reduce the uncertainty of the estimation. Here it is assumed that there is a relation between the flame area and the droplet area since the flame size depends on the amount of gaseous fuel coming from the droplet, as well as the droplet volume increases as the fuel evaporates. Moreover, the microdrops expelled from the main droplet were counted to determine the microexplosion frequency. As a result, the uncertainty of the ignition delay and microexplosion frequency were calculated as the standard deviation for each experimental condition.

In Table 3, the coefficient of variation (the ratio of the standard deviation to the mean) for the ignition delay and microexplosion

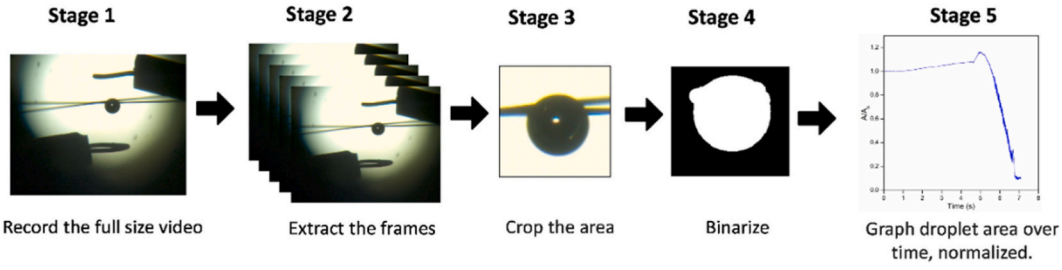

Fig. 4. Flow diagram of the algorithm for processing shadowgraph images.

Table 2
Highest, lowest, and average coefficient of variation of the ratio of the droplet area at any given time to the droplet area at the start of the heating (A/A_0).

Fuel/nanofuel	Coefficient of variation of A/A_0		
	Maximum	Minimum	Mean
Commercial diesel (B10)	28.5 %	0.002 %	1.6 %
Commercial diesel + Butanol (B10-Bu)	53.4 %	0.003 %	3.3 %
Commercial diesel + Butanol + CQD (B10-Bu-CQD)	73.1 %	0.02 %	4.1 %

frequency is presented to determine the uncertainty of these parameters for each fuel. The coefficient of variation for the ignition delay was found to be less than 2 %, signifying a reliable estimation for this parameter. However, the microexplosion frequency exhibited higher coefficients of variation due to the uncertainty in visualizing and counting micro drops. This is because microexplosions can occur in any direction from the main droplet, leading to some microdroplets being expelled on planes perpendicular to the camera's plane, making them unseen and uncounted. This is a limitation of the experimental technique used in this study.

3. Results

3.1. Characterization of the SCGs and CQD

Fig. 5a and b show an SEM micrograph and the TGA results of the SCGs, respectively. As observed, this material has an irregular shape and a rough surface. In addition, the TGA revealed weight loss at temperatures below 100 °C, which is attributed to water evaporation. The weight loss between 200 °C and 500 °C could be related to cellulose, hemicellulose, and lignin degradation [42]. Finally, the weight loss around 800 °C corresponds to the combustion of organic material.

Fig. 6 shows the TEM micrographs of the CQD. The micrographs reveal a quasi-spherical particle with an average size of 3.99 ± 1.58 nm. The d50 and d99 values of the CQD correspond to 3.43 nm and 7.71 nm, respectively. The CQD are formed through complex dehydration and condensation reactions of SCGs components during synthesis [43].

The chemical composition of the CQD was evaluated by EDS. The EDS spectrum of this material is shown in supplementary material, and it evidences the presence of carbon and oxygen. The presence of oxygen could be related to oxygen functionalities [44]. The XPS and FTIR analysis are shown in Fig. 7. Two representative peaks of C1s (284.5 eV) and O1s (532 eV) are present. The Si2p bands are related to the Si substrate [45]. The high-resolution XPS spectrum of C1s (Fig. 7b) evidenced the bands at 284.5 eV (C=C) [46], 285.6 eV (C-O) [47] and 288.9 eV (C=O) [48]. The O1s spectrum (Fig. 7c) exhibits three bands at 532 eV (C-OH) [49], 531.5 eV (C=O) [50], and 533 eV (C-O) [51,52]. FTIR analysis evidenced that bands between 3000 cm^{-1} and 3600 cm^{-1} correspond to the O-H functional group. The peaks at 2926 cm^{-1}, 2852 cm^{-1}, and 670 cm^{-1} are associated with the vibrations of the C-H functional group. Those at 1730 cm^{-1}, 1180 cm^{-1}, and 1050 cm^{-1} are due to the vibrations of the C=O functional group. That at 1650 cm^{-1} is associated with the vibration of the C=C functional group [53]. Finally, that at 1460 cm^{-1} is due to the vibration of the C-C functional group [54]. The XPS and FTIR confirmed the presence of sp^2 (C=C) and sp^3 carbon hybridizations [55]. The sp^3 carbons are related to oxygen functionalities on the CQD surface. These functional groups could have interesting effects on their optical and thermal properties.

Fig. 8 shows the optical properties of the CQD. The CQD's UV–Vis absorption spectrum (Fig. 8a) evidenced three bands at 224, 280, and 330 nm. The absorbance band at 224 nm is related to $\pi \rightarrow \pi^*$ transition of the C=C bonds [56], and those at 280 and 330 nm correspond to the n-π^* transition of the C=O bonds [56,57]. The insert in Fig. 8a shows an image of the n-butanol and the n-butanol-CQD samples under UV light irradiation. The blue light emitted by the CQD could be related to the presence of oxygenated functional groups, creating different discrete sp^2 energy levels between the states and π and π^* bands [58], supported by the FTIR spectrum of the CQD.

Fig. 8b depicts the CQD's photoluminescence (PL) with excitation wavelength variations ranging from 320 to 420 nm. The most significant emission peak was observed at 460 nm when an excitation wavelength of 370 nm was used.

The PL in CQD may be related to the isolation of sp^2 domains by sp^3 domains. The sp^3 domains are formed due to oxygen functionalities, as evidenced by the CQD's FTIR and UV–Vis spectra. Furthermore, the emission behavior depending on the excitation wavelength could be due to the presence of oxygen functionalities that cause surface defects, which act as surface energy traps [59–61]. This suggests that the chemical composition of the CQD controls their PL. Oxygen functionalities on the CQD surface can improve diesel fuel efficiency [62].

Table 3
The coefficient of variation for the ignition delay of each fuel tested.

Fuel/nanofuel	Coefficient of variation of the ignition delay	Coefficient of variation of the microexplosion frequency
Commercial diesel (B10)	1.0 %	21.5 %
Commercial diesel + Butanol (B10-Bu)	1.7 %	35.8 %
Commercial diesel + Butanol + CQD (B10-Bu-CQD)	1.7 %	24.0 %

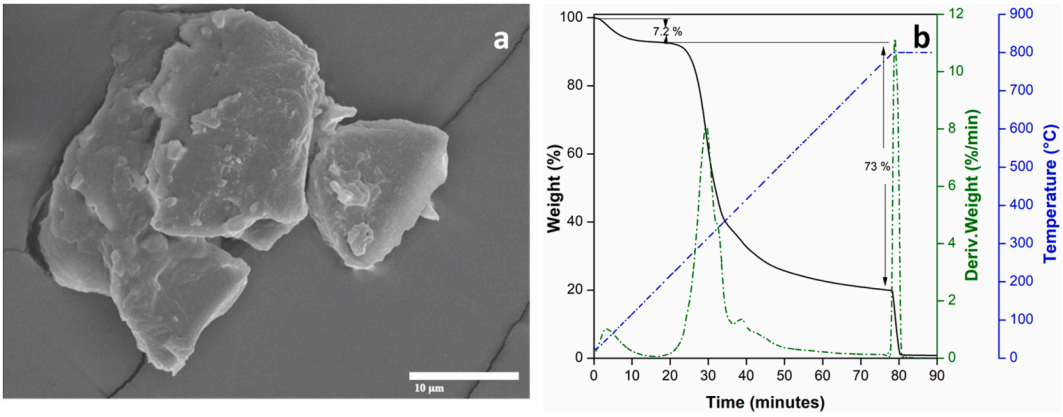

Fig. 5. (a) SEM micrograph and (b) TGA results of the spent coffee grounds.

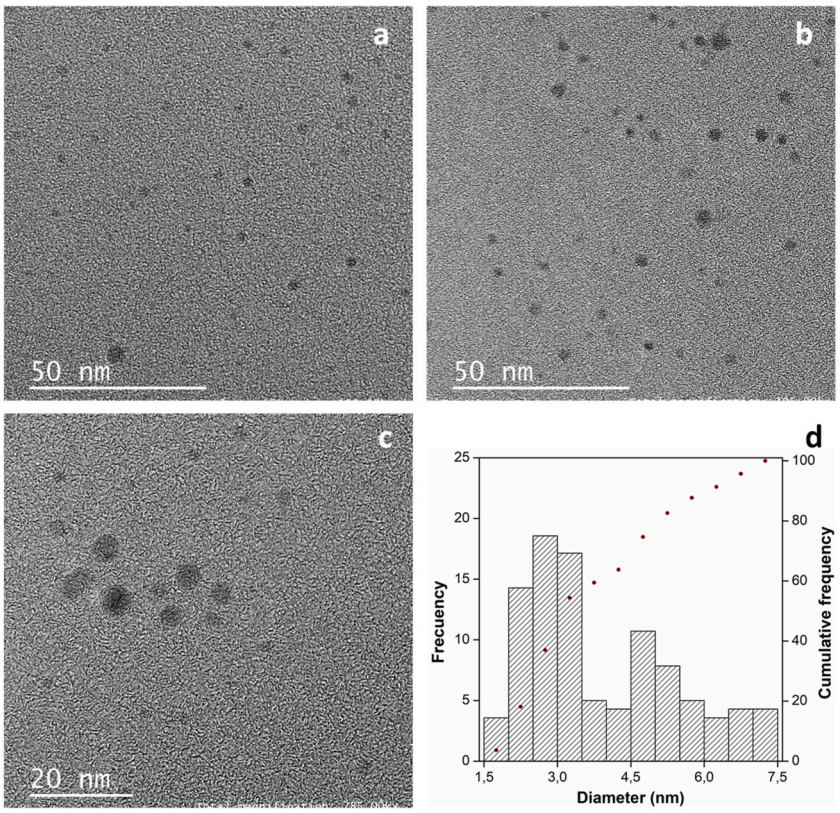

Fig. 6. TEM micrographs of the carbon quantum dots obtained from spent coffee grounds (a–c), Particle size distribution (b).

3.2. Ignition delay

The ignition delay of individual liquid fuel droplets is a combustion parameter that determines the time between the introduction of the fuel droplet into the hot atmosphere and its eventual ignition [63]. A decrease in ignition delay is considered beneficial for the environmental performance of combustion equipment since it reduces NO_x emissions [37], as there is less fuel accumulation during the premixed combustion stage, although these emissions could increase due to a higher combustion temperature as a consequence of a more efficient combustion. On the contrary, a longer ignition delay provides more time for the mixing of fuel and air, which favors lean combustion and higher temperatures of the reaction [64], and consequently, a decrease in particulate matter and an increase in NOx emissions are expected.

However, advanced engine technology nowadays includes techniques like Exhaust Gas Recirculation (EGR), which controls NOx

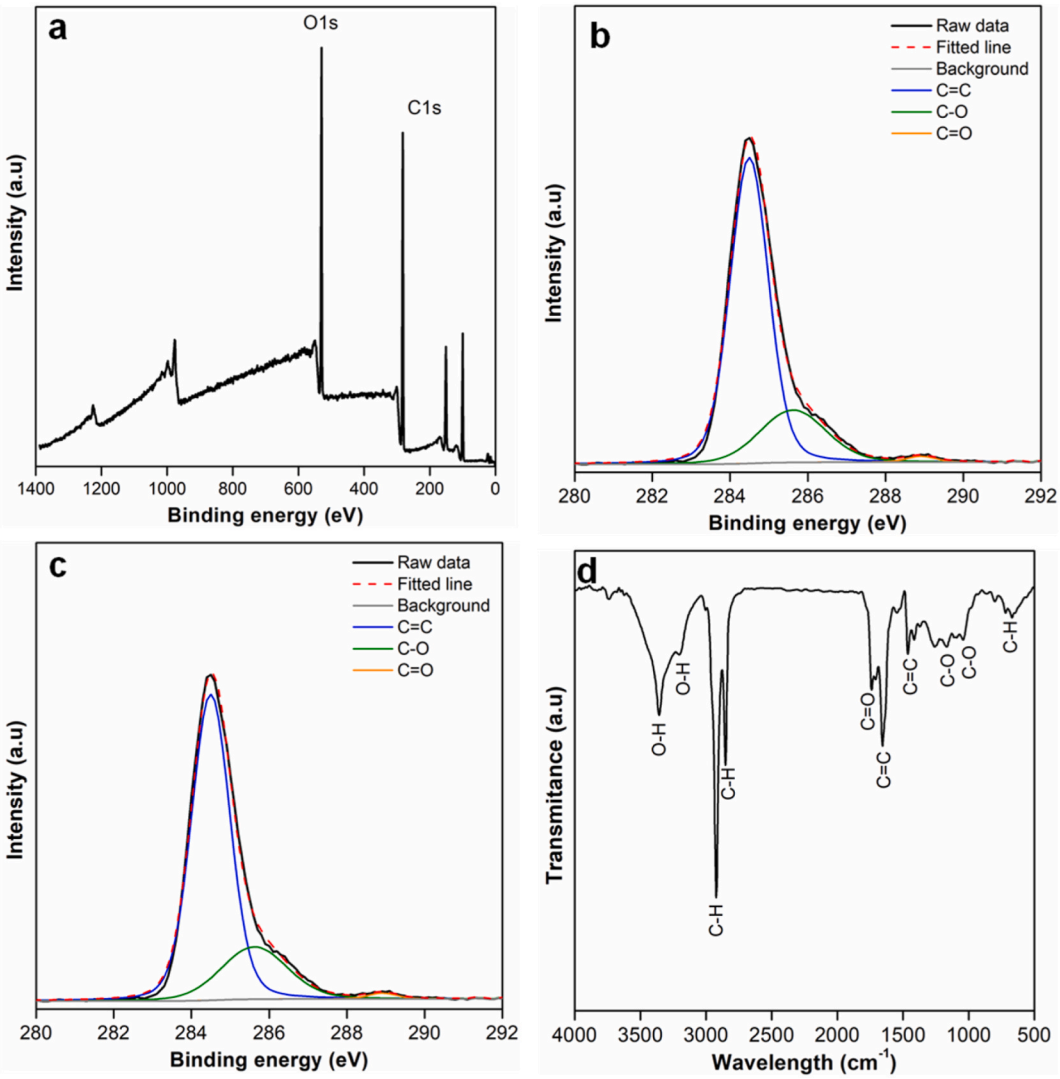

Fig. 7. (a) XPS survey spectrum, b) High-resolution XPS of the C1s, c) High-resolution XPS of the O1s, d) FTIR spectrum of CQD.

emissions. Therefore, these devices can withstand an operation with a larger ignition delay and keep emissions of particulate matter and NOx under allowed levels. Ignition delay also affects the performance of an Ignition Compression Engine because a lower ignition delay avoids early ignition since fuels with lower cetane numbers have longer ignition delays [65].

Fig. 9 shows the transient variation of the normalized area (A/A_0) of B10, B10-Bu, and B10-Bu-CQD. The first part of the curves corresponds to the evaporation of the fuel before the ignition and combustion. The three fuels had a similar evaporation stage between 0 and 4.5 s approximately, but there were differences at the beginning of the combustion. Fig. 10 shows the comparison of ignition delay for every experimental condition. Ignition delay was calculated as the time where the normalized area (A/A_0) is 95 % of the maximum for every curve in Fig. 9 [41]. B10 has the lower ignition delay, which was 5.4 % and 16.5 % lower than the ignition delay of B10-Bu and B10-Bu-CQD, respectively. These differences were significant according to the comparison of means with 95 % confidence intervals using the Tukey test shown in Fig. 11.

Regarding the trends in Fig. 9, unlike the blends containing butanol, the B10 droplet showed a smooth variation during combustion, related to homogeneous evaporation and combustion, where the droplet's shape mainly remained spherical. This indicates stable combustion of B10, and it is likely to follow the classical d^2-law. B10-Bu and B10-Bu-CQD blends had a similar trend during the combustion stage, where a series of fluctuations of the droplet area can be seen from the beginning to the end of the combustion. These fluctuations during the droplet combustion are due to the contraction and expansion of the droplet because there is an internal phase circulation of butanol and CQD to the droplet's surface, creating a layer with a high surface tension [66]. This higher surface tension retains the vapor of butanol and diesel in the droplet formed by the heating coming from the flame envelope, and the droplet expands until the internal pressure of the vapor overcomes the surface tension and leaves the droplet. Once the vapor is released, the droplet contracts and the formation of vapor within the droplet begins again. This cycle continues throughout the combustion, causing

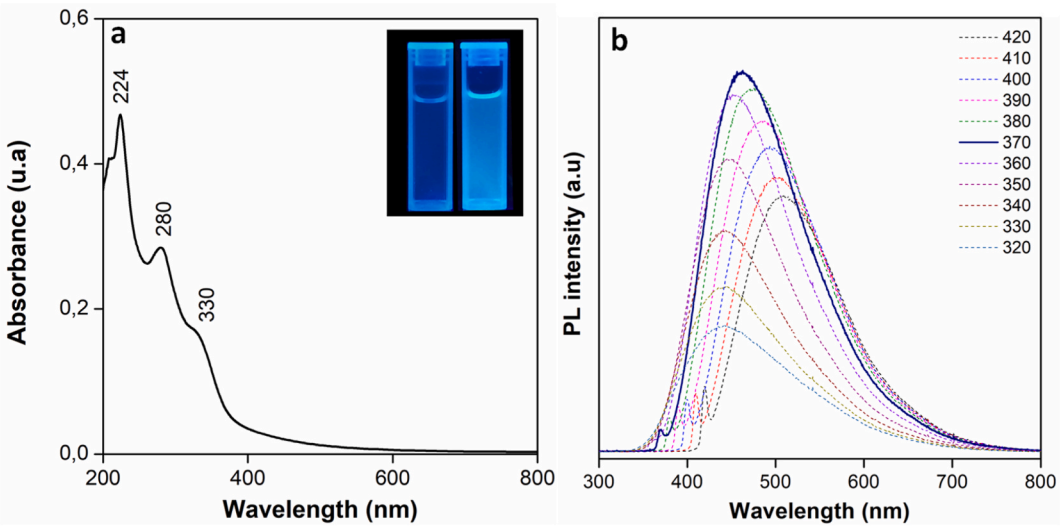

Fig. 8. Optical properties of the carbon quantum dots: (a) UV–Vis spectrum and (b) photoluminescence.

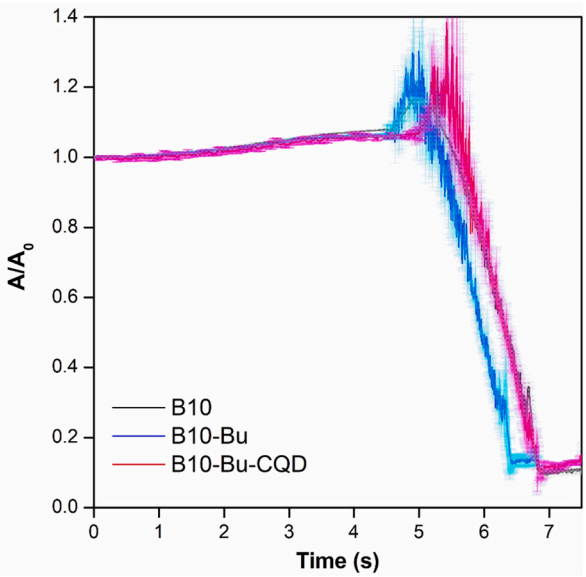

Fig. 9. Variation of the normalized area of the droplet during evaporation and combustion of B10 and the blends of B10 with Butanol and CQD.

fluctuations in the droplet area.

It is well known that the ignition delay consists of both physical and chemical components. The physical delay is attributed to the time required for fuel evaporation and the formation of flammable mixtures with air, while the chemical delay is due to precombustion reactions between fuel and air. In the context described, the enhanced resistance to evaporation resulting from the transport of butanol and CQD to the droplet surface necessitates more energy to form a combustible mixture with air. Consequently, the ignition delay, as illustrated in Fig. 10, increases due to the prolonged physical delay time. The presence of CQD has a significant impact on the physical ignition delay due to two main effects: 1) CQD can decrease the droplet evaporation rate by gradually forming a semi-solid porous crust of weakly bound micro-scale agglomerates, which inhibits internal liquid fuel diffusion, and 2) the formation of a porous shell as a result of vaporization and an increase in surface concentration of the nanophase impedes the movement of the internally trapped liquid core towards the droplet surface, thus reducing its evaporation and, consequently, the burning rate [67]. As a result, droplets containing CQD require more energy for the vapor to be expelled to mix with air in the droplet envelope, leading to an increase in physical ignition delay. On the other hand, the cetane number of butanol is approximately 44–55 % lower than that of diesel [68]. Since the cetane number measures fuel reactivity [69], a lower cetane number resulting from the combination of diesel and butanol reduces the blend's reactivity, which is heavily dependent on precombustion reactions between the fuel and air. Therefore, the addition of butanol

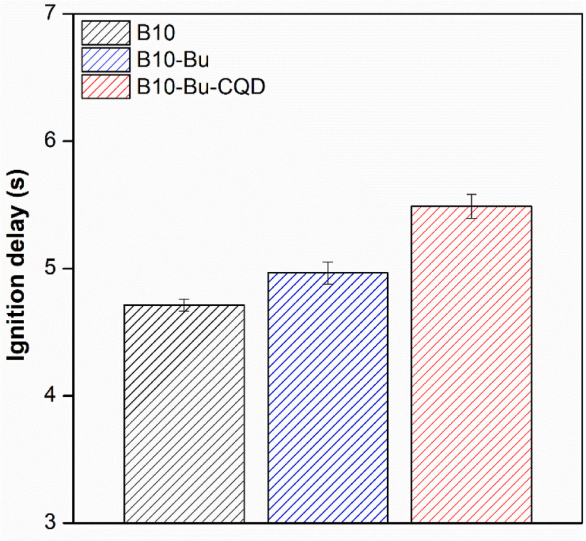

Fig. 10. Ignition delay during combustion of droplets of commercial diesel (B10), blend diesel–butanol (B10-Bu), and blend diesel–butanol-CQD (B10-Bu-CQD).

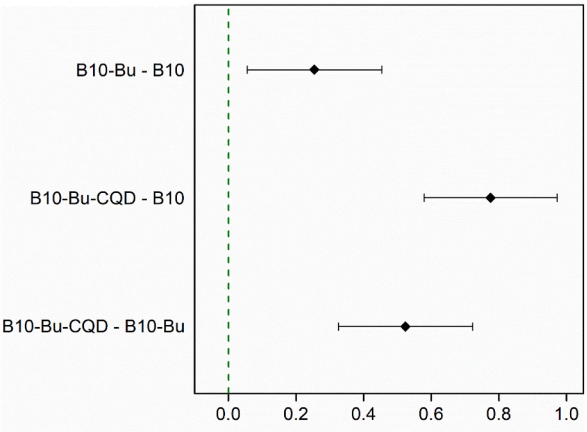

Fig. 11. 95 % Tukey confidence intervals comparing the ignition delay of the tested fuels (If an interval does not contain zero, the corresponding means are significantly different).

to B10 increases the chemical delay, and according to what was discussed previously, both higher physical and chemical delays contribute to the more significant ignition delay of B10-Bu and B10-Bu-CQD compared to B10.

The fact that blends of B10 with butanol and CQD have a higher ignition delay than B10 directly affects their use in Ignited Compression Engines, as it may cause an increase in the premixed stage of the combustion and a higher temperature of the reaction. This increase in temperature allows for the reduction of particulate matter and unburned hydrocarbon emissions, but it may have an adverse effect on the NOx emissions. On the other hand, a longer ignition delay promotes a more homogeneous mixing between air and fuel, which can lead to faster combustion than in a diffusion regime.

3.3. Microexplosions

Microexplosion is a phenomenon in which a fuel droplet breaks up into numerous smaller droplets of varying sizes. This process triggers rapid decomposition or secondary atomization of the fuel droplet, leading to rapid fuel evaporation, an increase in the burning area of droplets, and improved utilization of surrounding oxygen. It's worth noting that as the density and frequency of micro-explosions increase, the lifetime of the droplets generally decreases [68]. This, in turn, promotes better mixing of fuel and air within the engine combustion chamber, ultimately enhancing combustion. Consequently, it is possible to reduce emissions of CO, unburned hydrocarbons, particulate matter, as well as to improve fuel consumption, as the intensity of micro-explosions directly correlates with higher droplet combustion efficiency [70].

In this study, the frequency of microexplosion was determined by counting the number of microdroplets detached from a drop during its combustion period. The detachment was captured using a high-speed camera, as producing microdroplets during combustion is a random process. Based on this count, the ratio of microdroplets ejected from the main drop to the observation time was calculated. Fig. 12 shows the results obtained from the microexplosion frequency of the different fuel blends compared to B10.

Fig. 13 compares the means of microexplosion frequency with their 95 % confidence intervals using the Tukey test. The results showed that the B10-Bu blend had an average increase of 337 % compared to B10. However, adding CQD to the blend showed no significant increase compared to the B10-Bu mixture. Only the increase with butanol addition was statistically significant, as indicated in the comparison of means.

It has been found that microexplosions occur less frequently when droplets have a uniform boiling point throughout, and they may occur during the final stages of combustion for some droplets due to uneven heating while evaporating [71]. The increase in micro-explosions in the B10-Butanol blend is mainly caused by the lower boiling point of butanol, which is lower than that of diesel. The difference in volatility of fuel components leads to the formation of butanol bubbles within the mixture droplet as it heats up from the surrounding flame. This occurs because components with varying volatilities, which are preferentially retained in the center of the droplet, enter the vapor phase, causing an increase in internal pressure. As a result, the droplet inflates and contracts, resulting in a constant change in droplet diameter [72]. Due to the boiling that takes place on the surface of the droplet, the droplet contracts and expands, forming necks and leading to the creation of smaller daughter droplets [66]. Additionally, the trapping of volatile components within the rapidly heated droplet interior can initiate homogeneous or heterogeneous nucleation [73], i.e, this nucleation can occur away from the surface of the droplet or in the interface air-droplet, and it could potentially result in the fragmentation of the parent droplet due to internal pressure buildup.

The formation and collapse of bubbles during droplet combustion disrupt the droplet's geometry, causing it to expand and contract at different times, as illustrated in Fig. 14. This leads to non-linear reduction of droplet diameter over time and deviates from the classical D^2-law. Although the microexplosions and droplet surface oscillations were not strong enough to decompose the flame outside the droplet, they could result in flame instabilities on a larger scale due to the disruption of the combustion process and inefficient atomization [66]. Despite this, the continuous expansion and collapse of the droplet decreases its size and lifetime, leading to an increase in its effective surface area. As a result, this accelerates mixing with air [64,74].

In Fig. 15, it is made a qualitative comparison of the microexplosion frequency of B10, B10-Butanol, and B10-Butanol CQD. The results show that adding CQD did not significantly affect the average frequency of microexplosions compared to B10, as previously observed in Fig. 12. However, when compared to the B10-Butanol blend, the microexplosion frequency was lower, even when the blend contained butanol and CQD. Hence, CQD played a role as an inhibitor of microexplosion formation despite displaying a cycle of expansion and contraction like the B10-Bu blend.

To understand this phenomenon, it is important to note that nanoparticles, such as CQD, tend to agglomerate through orthokinetic and perikinetic mechanisms. To understand this phenomenon, it is important to note that nanoparticles, such as CQD, tend to agglomerate through orthokinetic and perikinetic mechanisms. The resultant agglomerates drive the droplet into an irregular inflation/deflation cycle by raising the concentration of particles in the droplet surface and producing a type of membrane that maintains the internal pressure build-up with bubbles trapped in the viscous core [67]. This causes an expected reduction in the bubble ejection frequency with droplet-shape oscillations, i.e., there is a reduction in the number of microexplosions in comparison to the blend with only butanol under the same heating conditions. This mechanism has also been observed previously in the combustion of titanium and ethanol-water blends [75]. On the other hand, Migliani et al. [67] also suggested that the suspended nanophase, in this case, the CQD agglomerates, could serve as potential nucleation sites when exposed to volumetric heating from the surrounding flame envelope. This transition from homogeneous to heterogeneous nucleation mechanisms leads to a decrease in the degree of accumulated excess superheat and, consequently, internal pressure build-up within the droplet. As a result, this facilitates a reduction in the intensity of microexplosions in the B10-Bu-CQD blend compared with the B10-Bu one.

It is important to note that the droplet's expansion and contraction cycles followed a similar pattern to that of the B10-Butanol blend during combustion (see Fig. 9). This similarity was observed despite the lower frequency of micro-explosions with the B10-Bu-CQD blend. This may be because of the higher density of nucleation sites formed by the CQD, which increases the possibility of bubble coalescence and growth. However, CQD inhibits micro-explosions' formation, which can help maintain flame stability since such events must occur at low intensities to keep the flame stable [76]. In this study, the synthesized CQD contains oxygen in its structure. Hence, moderate micro-explosions can transport these CQD to the flame and provide additional oxygen, which helps to complete soot oxidation and unburned fuel. Therefore, it is worth investigating the use of B10-Bu-CQD in internal compression engines to assess its effects on a larger scale.

Finally, the scope of this study is limited to the use of a single concentration of CQD, obtained directly from processing spent coffee grounds via solvothermal method. Although it has been noted that the presence of CQD affects ignition delay and microexplosion frequency, it is important to understand how changes in CQD concentration can impact these properties. Furthermore, the experimental method does not allow for the determination of chemical ignition delay or the precise measurement of ignition time, as OH radicals were not measured.

4. Conclusions

The use of additives is increasingly popular in internal combustion engines as they could enhance engine efficiency and decrease pollutant emissions. In this research, Carbon Quantum Dots were synthesized from Spent Coffee Grounds through a solvothermal method using n-butanol as a solvent. The presence of CQD in n-butanol was confirmed through TEM analysis, and the oxygen

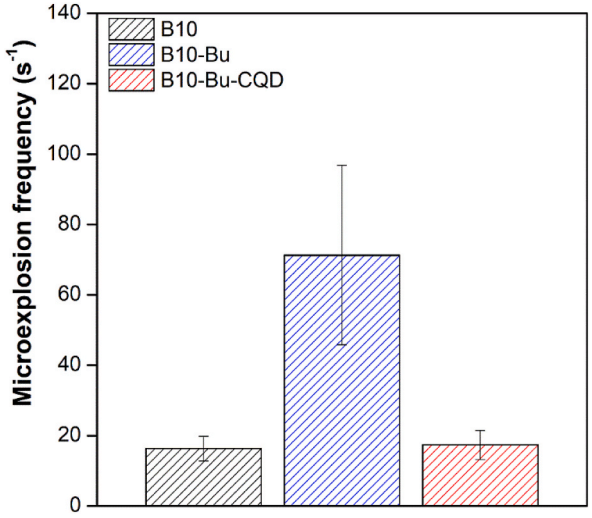

Fig. 12. Microexplosion frequency during combustion of droplets of commercial diesel (B10), blend diesel–butanol (B10-Bu), and blend diesel–butanol-CQD (B10-Bu-CQD).

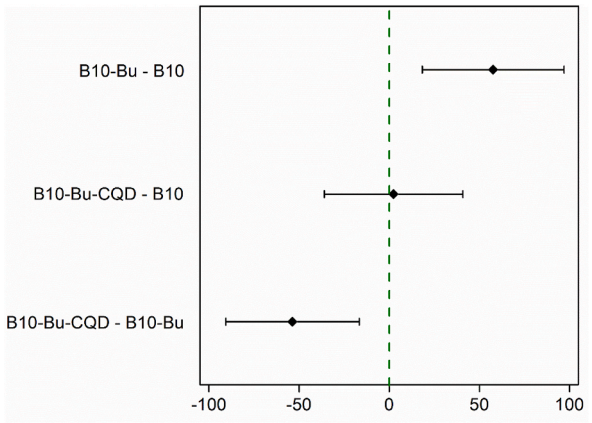

Fig. 13. 95 % Tukey confidence intervals comparing the microexplosion frequency of the tested fuels. (If an interval does not contain zero, the corresponding means are significantly different.)

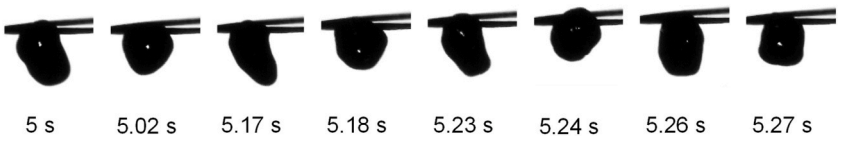

Fig. 14. Expansion and contraction of a droplet of diesel-butanol blend during combustion.

functionalities were identified using FTIR and XPS. The CQD in n-butanol was employed as an additive to commercial diesel, and its combustion performance was assessed at the droplet scale.

When n-butanol and n-butanol-CQD were added to commercial diesel, it caused an increase in ignition delay by 5.6 % and up to 16.5 %, respectively. This happened because n-butanol and CQD accumulated on the droplet surface, increasing the vaporization heat required to initiate combustion. This, in turn, caused droplet surface oscillations, making combustion unstable. However, the presence of CQD on the droplet surface reduced the number of micro-explosions caused by the increased internal pressure of boiling n-butanol.

The blend B10-Bu-CQD has a micro-explosion frequency like that of B10 and is more than three times lower than the blend B10-n-butanol. Therefore, CQD can promote fuel evaporation by increasing the density of nucleation sites for bubble formation and preventing micro-explosions, resulting in stable combustion.

These characteristics can significantly impact the performance of blends in Compression Ignited Engines. However, more research

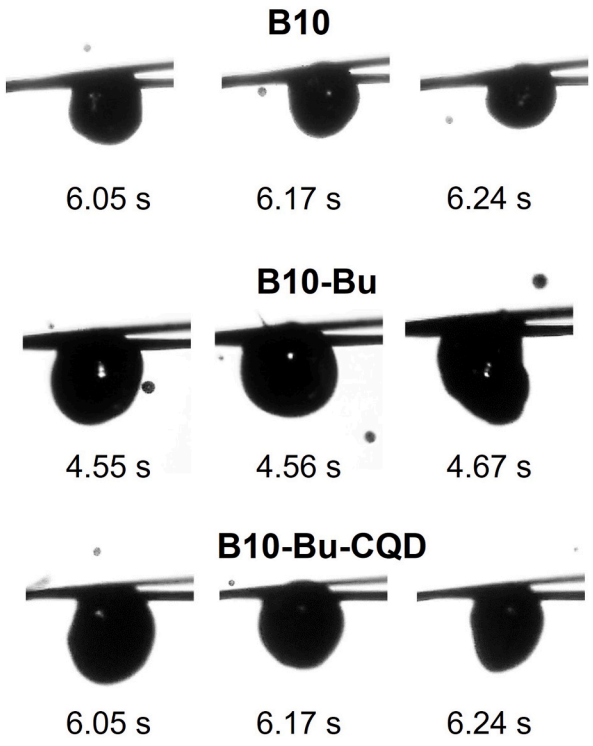

Fig. 15. Qualitative comparison of the microexplosion frequency with B10, B10-Bu, and B10-Bu-CQD.

is required to determine the impact of these nanofuels on pollutant formation, fuel injection, and ignition delay in engines.

CRediT authorship contribution statement

C. Zapata-Hernandez: Writing – original draft, Methodology, Formal analysis, Data curation, Conceptualization. **G. Durango-Giraldo:** Methodology, Investigation, Data curation. **Miguel Gomez-Echeverri:** Visualization, Methodology, Investigation, Data curation. **R. Buitrago-Sierra:** Writing – review & editing, Investigation, Formal analysis, Conceptualization. **Bernardo Herrera:** Writing – review & editing, Methodology, Investigation, Formal analysis, Conceptualization. **Karen Cacua:** Writing – review & editing, Supervision, Project administration, Methodology, Investigation, Formal analysis, Conceptualization.

Declaration of generative AI and AI-assisted technologies in the writing process

During the preparation of this work the author(s) used Grammarly, Inc. to improve the language and readability of the manuscript. After using this tool/service, the author(s) reviewed and edited the content as needed and takes full responsibility for the content of the publication.

Declaration of competing interest

The authors declare that they have no known competing financial interests or personal relationships that could have appeared to influence the work reported in this paper.

Acknowledgments

The authors would like to thank the Ministry of Science, Technology, and Innovation in Colombia (abbreviated Minciencias in Spanish) for financing the research program entitled “Use of carbon nanomaterials as additives in diesel for internal combustion engines working in dual mode with natural gas and their effects on yield, pollutant emissions, and cell damage” under project No. 70848.

Appendix A. Supplementary data

Supplementary data to this article can be found online at https://doi.org/10.1016/j.heliyon.2024.e39671.

List of abbreviations

CQD Carbon Quantum Dots
SCGs Spent Coffee Grounds
FE-SEM Field Emission Scanning Electron Microscopy
FTIR Fourier Transform Infrared
EDS Energy Dispersive X-ray Spectroscopy
TEM Transmission Electron Microscopy
TGA Thermogravimetric Analysis
ICE Internal Combustion Engines
CI engine: Compression Ignition Engine
PM Particulate Matter
DPF Diesel Particulate Filters
CNTs Carbon Nanotubes
GO Graphene Oxide
PL: Photoluminescence
XPS X-ray Photoelectron Spectroscopy
B10 Commercial diesel (diesel 90 % v/v and biodiesel 10 % v/v)
Bu-CQD CQD dispersed in n-butanol
B10-Bu Commercial diesel + Butanol (10 % v/v)
B10-Bu-CQD Commercial diesel + Butanol + CQD

References

[1] A.I. EL-Seesy, M.S. Waly, Z. He, H.M. El-Batsh, A. Nasser, R.M. El-Zoheiry, Enhancement of the combustion and stability aspects of diesel-methanol-hydrous methanol blends utilizing n-octanol, diethyl ether, and nanoparticle additives, J. Clean. Prod. 371 (Oct) (2022), https://doi.org/10.1016/j.jclepro.2022.133673.

[2] A. Pugazhendhi, et al., Biobutanol as a promising liquid fuel for the future - recent updates and perspectives, Fuel 253 (Oct. 2019) 637–646, https://doi.org/10.1016/j.fuel.2019.04.139.

[3] D. Fernández-Rodríguez, M. Lapuerta, L. German, Progress in the use of biobutanol blends in diesel engines, Energies 14 (11) (Jun. 01, 2021), https://doi.org/10.3390/en14113215. MDPI AG.

[4] Z. Zhang, et al., Investigation on combustion, performance and emission characteristics of a diesel engine fueled with diesel/alcohol/n-butanol blended fuels, Fuel 320 (Jul) (2022), https://doi.org/10.1016/j.fuel.2022.123975.

[5] V.B.M. Vinod Babu, M.M.K. Madhu Murthy, G. Amba Prasad Rao, Butanol and pentanol: the promising biofuels for CI engines – a review, Renew. Sustain. Energy Rev. 78 (2017) 1068–1088, https://doi.org/10.1016/j.rser.2017.05.038. Elsevier Ltd.

[6] Z. Chen, Z. Wu, J. Liu, C. Lee, Combustion and emissions characteristics of high n-butanol/diesel ratio blend in a heavy-duty diesel engine and EGR impact, Energy Convers. Manag. 78 (Feb. 2014) 787–795, https://doi.org/10.1016/j.enconman.2013.11.037.

[7] Y. Zhang, et al., A comprehensive review on combustion, performance and emission aspects of higher alcohols and its additive effect on the diesel engine, Fuel 335 (Mar. 01, 2023), https://doi.org/10.1016/j.fuel.2022.127011. Elsevier Ltd.

[8] M. Lapuerta, J.J. Hernández, D. Fernández-Rodríguez, A. Cova-Bonillo, Autoignition of blends of n-butanol and ethanol with diesel or biodiesel fuels in a constant-volume combustion chamber, Energy 118 (Jan. 2017) 613–621, https://doi.org/10.1016/j.energy.2016.10.090.

[9] S. Pan, et al., Discussion on the combustion, performance and emissions of a dual fuel diesel engine fuelled with methanol-based CeO2 nanofluids, Fuel 302 (Oct) (2021), https://doi.org/10.1016/j.fuel.2021.121096.

[10] Q. Chen, C. Wang, K. Shao, Y. Liu, X. Chen, Y. Qian, Analyzing the combustion and emissions of a DI diesel engine powered by primary alcohol (methanol, ethanol, n-butanol)/diesel blend with aluminum nano-additives, Fuel 328 (Nov) (2022), https://doi.org/10.1016/j.fuel.2022.125222.

[11] D. Firew, R.B. Nallamothu, G. Alemayehu, R. Gopal, Performance and emission evaluation of CI engine fueled with ethanol diesel emulsion using NiZnFe2O4 nanoparticle additive, Heliyon 8 (11) (Nov. 2022) e11639, https://doi.org/10.1016/j.heliyon.2022.e11639.

[12] G. Pullagura, et al., Performance, combustion and emission reduction characteristics of Metal-based silicon dioxide nanoparticle additives included in ternary fuel (diesel-SMME-iso butanol) on diesel engine, Heliyon 10 (4) (Feb. 2024) e26519, https://doi.org/10.1016/j.heliyon.2024.e26519.

[13] E. Ettefaghi, et al., Bio-nano emulsion fuel based on graphene quantum dot nanoparticles for reducing energy consumption and pollutants emission, Energy 218 (Mar) (2021), https://doi.org/10.1016/j.energy.2020.119551.

[14] N. Chacko, T. Jeyaseelan, Comparative evaluation of graphene oxide and graphene nanoplatelets as fuel additives on the combustion and emission characteristics of a diesel engine fuelled with diesel and biodiesel blend, Fuel Process. Technol. 204 (Jul) (2020), https://doi.org/10.1016/j.fuproc.2020.106406.

[15] T. Kegl, A. Kovač Kralj, B. Kegl, M. Kegl, Nanomaterials as fuel additives in diesel engines: a review of current state, opportunities, and challenges, Prog. Energy Combust. Sci. 83 (2021), https://doi.org/10.1016/j.pecs.2020.100897.

[16] A. Heidari-Maleni, T.M. Gundoshmian, B. Karimi, A. Jahanbakhshi, B. Ghobadian, A novel fuel based on biocompatible nanoparticles and ethanol-biodiesel blends to improve diesel engines performance and reduce exhaust emissions, Fuel 276 (April) (2020) 118079, https://doi.org/10.1016/j.fuel.2020.118079.

[17] A. Taheri-Garavand, A. Heidari-Maleni, T. Mesri-Gundoshmian, O.D. Samuel, Application of artificial neural networks for the prediction of performance and exhaust emissions in IC engine using biodiesel-diesel blends containing quantum dot based on carbon doped, Energy Convers. Manag. X 16 (Dec) (2022), https://doi.org/10.1016/j.ecmx.2022.100304.

[18] A. Heidari-Maleni, T. Mesri-Gundoshmian, A. Jahanbakhshi, B. Karimi, B. Ghobadian, Novel environmentally friendly fuel: the effect of adding graphene quantum dot (GQD) nanoparticles with ethanol-biodiesel blends on the performance and emission characteristics of a diesel engine, NanoImpact 21 (May 2020) (2021) 100294, https://doi.org/10.1016/j.impact.2021.100294.

[19] H. Değirmenci, R. Küçükosman, A. Alper Yontar, An experimental study on droplet-scale combustion and atomization behavior in pure ethanol, methanol, and trimethyl borate, and their blends, Fuel 357 (Feb) (2024), https://doi.org/10.1016/j.fuel.2023.129716.

[20] B. Huang, X. Yang, Y. Zhang, H. Zhang, W. Li, Y. Li, Characterizing bubble dynamics in combustion and atomization of alcohol/PODE4 and alcohol/n-undecane binary droplets, Fuel 352 (Nov) (2023), https://doi.org/10.1016/j.fuel.2023.129029.

[21] B. Huang, X. Yang, Y. Zhang, H. Zhang, W. Li, Y. Li, Characterizing combustion and atomization of PODEn and ethanol/PODEn binary droplets, Fuel 341 (Jun) (2023), https://doi.org/10.1016/j.fuel.2023.127672.
[22] X. Xi, H. Liu, C. Cai, M. Jia, X. Ma, Analytical and experimental study on boiling vaporization and multi-mode breakup of binary fuel droplet, Int J Heat Mass Transf 165 (Feb) (2021), https://doi.org/10.1016/j.ijheatmasstransfer.2020.120620.
[23] K. Han, B. Pang, C. Zhao, Z. Ni, Z. Qi, An experimental study of the puffing and evaporation characteristics of acetone–butanol–ethanol (ABE) and diesel blend droplets, Energy 183 (Sep. 2019) 331–340, https://doi.org/10.1016/j.energy.2019.06.068.
[24] R. Küçükosman, A.A. Yontar, K. Ocakoglu, Experimental studies on combustion and atomization characteristics of aliphatic and aromatic hydrocarbons droplets, J. Energy Inst. 108 (Jun) (2023), https://doi.org/10.1016/j.joei.2023.101249.
[25] D. Ozyurt, M. Al Kobaisi, R.K. Hocking, B. Fox, Properties, synthesis, and applications of carbon dots: a review, Carbon Trends 12 (Sep. 01, 2023), https://doi.org/10.1016/j.cartre.2023.100276. Elsevier Ltd.
[26] R. Atchudan, T.N. Jebakumar Immanuel Edison, M. Shanmugam, S. Perumal, T. Somanathan, Y.R. Lee, Sustainable synthesis of carbon quantum dots from banana peel waste using hydrothermal process for in vivo bioimaging, Physica E Low Dimens Syst Nanostruct 126 (2021) 114417, https://doi.org/10.1016/j.physe.2020.114417. August 2020.
[27] R.S. Tade, P.O. Patil, Green synthesis of fluorescent graphene quantum dots and its application in selective curcumin detection, Curr. Appl. Phys. 20 (11) (2020) 1226–1236, https://doi.org/10.1016/j.cap.2020.08.006.
[28] M. Xue, et al., Dual functionalized natural biomass carbon dots from lychee exocarp for cancer cell targetable near-infrared fluorescence imaging and photodynamic therapy, Nanoscale 10 (38) (2018) 18124–18130, https://doi.org/10.1039/c8nr05017a.
[29] H. Xu, L. Xie, M. Hakkarainen, Coffee-Ground-derived quantum dots for aqueous processable nanoporous graphene membranes, ACS Sustain Chem Eng 5 (6) (2017) 5360–5367, https://doi.org/10.1021/acssuschemeng.7b00663.
[30] J. McNutt, Q. Sophia He, Spent coffee grounds: a review on current utilization, J. Ind. Eng. Chem. 71 (Korean Society of Industrial Engineering Chemistry) (2019) 78, https://doi.org/10.1016/j.jiec.2018.11.054, 88, Mar. 25.
[31] S.I. Mussatto, E.M.S. Machado, S. Martins, J.A. Teixeira, Production, composition, and application of coffee and its industrial residues, Food Bioprocess Technol. 4 (5) (Jul. 2011) 661–672, https://doi.org/10.1007/s11947-011-0565-z.
[32] S.K. Karmee, A spent coffee grounds based biorefinery for the production of biofuels, biopolymers, antioxidants and biocomposites, Waste Management 72 (Feb. 01, 2018) 240–254, https://doi.org/10.1016/j.wasman.2017.10.042. Elsevier Ltd.
[33] C. Andrade, R. Perestrelo, J.S. Câmara, Bioactive compounds and antioxidant activity from spent coffee grounds as a powerful approach for its valorization, Molecules 27 (21) (Nov. 2022), https://doi.org/10.3390/molecules27217504.
[34] L. Yeoh, K.S. Ng, Future prospects of spent coffee ground valorisation using a biorefinery approach, Resour. Conserv. Recycl. 179 (Apr) (2022), https://doi.org/10.1016/j.resconrec.2021.106123.
[35] S. Thulasi, A. Kathiravan, M. Asha Jhonsi, Fluorescent carbon dots derived from vehicle exhaust soot and sensing of tartrazine in soft drinks, ACS Omega 5 (12) (Mar. 2020) 7025–7031, https://doi.org/10.1021/acsomega.0c00707.
[36] A. Mazzoli, O. Favoni, Particle size, size distribution and morphological evaluation of airborne dust particles of diverse woods by Scanning Electron Microscopy and image processing program, Powder Technol. 225 (Jul. 2012) 65–71, https://doi.org/10.1016/j.powtec.2012.03.033.
[37] J.B. Ooi, H.M. Ismail, V. Swamy, X. Wang, A.K. Swain, J.R. Rajanren, Graphite oxide nanoparticle as a diesel fuel additive for cleaner emissions and lower fuel consumption, Energy Fuel. 30 (2) (2016) 1341–1353, https://doi.org/10.1021/acs.energyfuels.5b02162.
[38] M.E.M. Soudagar, et al., Study of diesel engine characteristics by adding nanosized zinc oxide and diethyl ether additives in Mahua biodiesel–diesel fuel blend, Sci. Rep. 10 (1) (Dec. 2020), https://doi.org/10.1038/s41598-020-72150-z.
[39] F. Hussain, et al., Enhancement in combustion, performance, and emission characteristics of a diesel engine fueled with Ce-ZnO nanoparticle additive added to soybean biodiesel blends, Energies 13 (17) (Sep. 2020), https://doi.org/10.3390/en13174578.
[40] T. Wang, X. Qiao, T. Li, Y. Wei, Study on three droplet sequential burning characteristics of coal direct liquefied diesel, AIP Adv. 11 (4) (Apr. 2021), https://doi.org/10.1063/5.0046953.
[41] S. Mosadegh, A. Ghaffarkhah, C. van der Kuur, M. Arjmand, S. Kheirkhah, Graphene oxide doped ethanol droplet combustion: ignition delay and contribution of atomization to burning rate, Combust. Flame 238 (Apr) (2022), https://doi.org/10.1016/j.combustflame.2021.111748.
[42] P. Jagdale, D. Ziegler, M. Rovere, J.M. Tulliani, A. Tagliaferro, Waste coffee ground biochar: a material for humidity sensors, Sensors (Switzerland) 19 (4) (2019) 1–16, https://doi.org/10.3390/s19040801.
[43] S. Ding, Y. Gao, B. Ni, X. Yang, Green synthesis of biomass-derived carbon quantum dots as fluorescent probe for Fe 3 + detection, Inorg. Chem. Commun. 130 (2021) 108636, https://doi.org/10.1016/j.inoche.2021.108636. February 2020.
[44] S. Kumar, A.K. Ojha, B. Ahmed, A. Kumar, J. Das, A. Materny, Tunable (violet to green) emission by high-yield graphene quantum dots and exploiting its unique properties towards sun-light-driven photocatalysis and supercapacitor electrode materials, Mater. Today Commun. 11 (Jun. 2017) 76–86, https://doi.org/10.1016/j.mtcomm.2017.02.009.
[45] K. Liu, Y. Song, S. Chen, Oxygen reduction catalyzed by nanocomposites based on graphene quantum dots-supported copper nanoparticles, Int. J. Hydrogen Energy 41 (3) (Jan. 2016) 1559–1567, https://doi.org/10.1016/j.ijhydene.2015.10.059.
[46] N.A. Mahat, S.A. Shamsudin, Blue luminescence carbon quantum dots derived from oil palm empty fruit bunch biomass, in: IOP Conference Series: Materials Science and Engineering, Institute of Physics Publishing, Mar. 2020, https://doi.org/10.1088/1757-899X/736/5/052001.
[47] D. Li, et al., Supra-(carbon nanodots) with a strong visible to near-infrared absorption band and efficient photothermal conversion, Light Sci. Appl. 5 (7) (Jul. 2016), https://doi.org/10.1038/lsa.2016.120.
[48] C. Qi, H. Wang, A. Yang, X. Wang, J. Xu, Facile fabrication of highly fluorescent N-doped carbon quantum dots using an ultrasonic-assisted hydrothermal method: optical properties and cell imaging, ACS Omega 6 (48) (Dec. 2021) 32904–32916, https://doi.org/10.1021/acsomega.1c04903.
[49] Y. Gao, et al., An intelligent cooling material modified with carbon dots for evaporative cooling and UV absorption, Nanoscale Adv. 4 (19) (Aug. 2022) 4169–4174, https://doi.org/10.1039/d2na00380e.
[50] A. Tomskaya, I.P. Asanov, I. Yushina, M.I. Rakhmanova, S. Smagulova, Optical properties of tricarboxylic acid-derived carbon dots, ACS Omega 7 (48) (Dec. 2022) 44093–44102, https://doi.org/10.1021/acsomega.2c05503.
[51] S. Lin, et al., Solvatochromism of bright carbon dots with tunable long-wavelength emission from green to red and their application as solid-state materials for warm WLEDs, RSC Adv. 7 (66) (2017) 41552–41560, https://doi.org/10.1039/c7ra07736j.
[52] X. Jiang, et al., Synthesis of nitrogen-doped lignin/DES carbon quantum dots as a fluorescent probe for the detection of Fe3+ ions, Polymers 10 (11) (Nov. 2018), https://doi.org/10.3390/polym10111282.
[53] V. Ţucureanu, A. Matei, A.M. Avram, FTIR spectroscopy for carbon family study, Crit. Rev. Anal. Chem. 46 (6) (2016) 502–520, https://doi.org/10.1080/10408347.2016.1157013.
[54] Inamuddin, H. Abbas Kashmery, Polyvinylidene fluoride/sulfonated graphene oxide blend membrane coated with polypyrrole/platinum electrode for ionic polymer metal composite actuator applications, Sci. Rep. 9 (1) (2019) 1–11, https://doi.org/10.1038/s41598-019-46305-6.
[55] W.U. Khan, et al., High quantum yield green-emitting carbon dots for Fe(III) detection, biocompatible fluorescent ink and cellular imaging, Sci. Rep. 7 (1) (Dec. 2017), https://doi.org/10.1038/s41598-017-15054-9.
[56] N.A. Alarfaj, M.F. El-Tohamy, H.F. Oraby, CA 19-9 pancreatic tumor marker fluorescence immunosensing detection via immobilized carbon quantum dots conjugated gold nanocomposite, Int. J. Mol. Sci. 19 (4) (2018), https://doi.org/10.3390/ijms19041162.
[57] N. Architha, et al., Microwave-assisted green synthesis of fluorescent carbon quantum dots from Mexican Mint extract for Fe3+ detection and bio-imaging applications, Environ. Res. 199 (March) (2021) 111263, https://doi.org/10.1016/j.envres.2021.111263.
[58] N. Eun, J. Jeong, H. San, S. Yoon, S. Oh, Ultraviolet/blue light emitting high-quality graphene quantum dots and their biocompatibility, Carbon N Y 170 (2020) 213–219, https://doi.org/10.1016/j.carbon.2020.08.015.

[59] G.E. Lecroy, et al., Characteristic excitation wavelength dependence of fluorescence emissions in carbon 'quantum' dots, J. Phys. Chem. C 121 (50) (2017) 28180–28186, https://doi.org/10.1021/acs.jpcc.7b10129.
[60] H. Ding, X.H. Li, X.B. Chen, J.S. Wei, X.B. Li, H.M. Xiong, Surface states of carbon dots and their influences on luminescence, J. Appl. Phys. 127 (23) (2020), https://doi.org/10.1063/1.5143819.
[61] J.P. Malavika, C. Shobana, S. Sundarraj, M. Ganeshbabu, P. Kumar, R.K. Selvan, Green synthesis of multifunctional carbon quantum dots: an approach in cancer theranostics, Biomater. Adv. 136 (2022) 212756, https://doi.org/10.1016/j.bioadv.2022.212756. November 2021.
[62] S.S. Hoseini, G. Najafi, B. Ghobadian, M.T. Ebadi, R. Mamat, T. Yusaf, Performance and emission characteristics of a CI engine using graphene oxide (GO) nanoparticles additives in biodiesel-diesel blends, Renew. Energy 145 (2020) 458–465, https://doi.org/10.1016/j.renene.2019.06.006.
[63] S. Satcununathan, Ignition delay of individual liquid fuel droplets, Industrial & Engineering Chemistry Process Design and Delevelopment 10 (3) (1971) 297–304.
[64] M.R. Chow, et al., Effects of ethanol on the evaporation and burning characteristics of palm-oil based biodiesel droplet, J. Energy Inst. 98 (Oct. 2021) 35–43, https://doi.org/10.1016/j.joei.2021.05.008.
[65] S. Rabl, T.J. Davies, A.P. McDougall, R.F. Cracknell, Understanding the relationship between ignition delay and burn duration in a constant volume vessel at diesel engine conditions, Proc. Combust. Inst. 35 (3) (2015) 2967–2974, https://doi.org/10.1016/j.proci.2014.05.054.
[66] H. Değirmenci, R. Küçükosman, A. Alper Yontar, An experimental study on droplet-scale combustion and atomization behavior in pure ethanol, methanol, and trimethyl borate, and their blends, Fuel 357 (Feb) (2024), https://doi.org/10.1016/j.fuel.2023.129716.
[67] A. Miglani, S. Basu, R. Kumar, Insight into instabilities in burning droplets, Phys. Fluids 26 (3) (Feb. 2014), https://doi.org/10.1063/1.4866866.
[68] R. Küçükosman, A.A. Yontar, K. Ocakoglu, Experimental studies on combustion and atomization characteristics of aliphatic and aromatic hydrocarbons droplets, J. Energy Inst. 108 (Jun) (2023), https://doi.org/10.1016/j.joei.2023.101249.
[69] B. McGann, K. Kim, T. Lee, J. Temme, C.B. Kweon, Effect of the cetane number on jet fuel spray ignition at high-temperature and-pressure conditions, Energy Fuel. 34 (2) (Feb. 2020) 1337–1346, https://doi.org/10.1021/acs.energyfuels.9b03170.
[70] K. Meng, L. Bao, F. Li, C. Wang, Q. Lin, Experimental understanding on combustion and micro-explosion characteristics of mixed droplets of aviation fuel, biodiesel and ethanol, J. Energy Inst. 97 (Aug. 2021) 169–179, https://doi.org/10.1016/j.joei.2021.03.021.
[71] G. Zhang, et al., Acoustic excitation of an n-heptane droplet: evaporation, ignition and combustion characteristics, Aerosp Sci Technol 133 (Feb) (2023), https://doi.org/10.1016/j.ast.2023.108128.
[72] S. Basu, A. Miglani, Combustion and heat transfer characteristics of nanofluid fuel droplets: a short review, Int. J. Heat Mass Tran. 96 (May 01, 2016) 482–503, https://doi.org/10.1016/j.ijheatmasstransfer.2016.01.053. Elsevier Ltd.
[73] C.K. Law, Internal boiling and superheating in vaporizing muhicomponent droplets, AlChE Journal 24 (4) (1978) 626–632.
[74] X. Xi, H. Liu, C. Cai, M. Jia, X. Ma, Analytical and experimental study on boiling vaporization and multi-mode breakup of binary fuel droplet, Int J Heat Mass Transf 165 (Feb) (2021), https://doi.org/10.1016/j.ijheatmasstransfer.2020.120620.
[75] A. Miglani, S. Basu, Effect of particle concentration on shape deformation and secondary atomization characteristics of a burning nanotitania dispersion droplet, J. Heat Tran. 137 (10) (2015), https://doi.org/10.1115/1.4030394.
[76] R. Küçükosman, A.A. Yontar, K. Ocakoglu, Nanoparticle additive fuels: atomization, combustion and fuel characteristics, J. Anal. Appl. Pyrol. 165 (Aug. 01, 2022), https://doi.org/10.1016/j.jaap.2022.105575. Elsevier B.V.